Periodic Nanotemplating by Selective Deposition of Electroless Gold Island Films on Particle-Lithographed Dimethyldichlorosilane Layers

Wonmi Ahn[†] and D. Keith Roper[†,‡,*]

[†]Department of Materials Science and Engineering, 304 CME, University of Utah, Salt Lake City, Utah 84112 and [‡]Ralph E. Martin Department of Chemical Engineering, 3202 BELL Engineering Center, University of Arkansas, Fayetteville, Arkansas 72701

ABSTRACT Uniform hexagonal arrays of diverse nanotemplated metal structures were formed *via* selective electroless gold plating on particle-lithographed dimethyldichlorosilane layers. Surface-associated water at silica bead interstices was shown to correlate with the formation of silane rings with outer ring diameters ranging from 522.5 ± 29.7 to 1116.9 ± 52.6 nm and/or spherical gold nanoparticles with diameters from 145.5 ± 20.2 to 389.1 ± 51.1 nm in the array. Reproducibility and millimeter-size scalability of the array were achieved without the need for expensive and sophisticated lithography or metal deposition equipment. The formation of each structure was explained on the basis of the silanization mechanism and microscopic characterization, as well as dimensional analysis of the nanostructures. This new, facile, and versatile method enables fine fabrication of regular metal nanoparticle array platforms to improve optical and plasmonic features in nanoelectronics and nanophotonic devices.

KEYWORDS: particle lithography · silanization · electroless plating · nanotemplating · gold island thin film

Metallic nanostructures in a regular arrangement are important not only in fundamental sciences[1] but also in many applications because they create stronger resonant electromagnetic (EM) surface wave energy coupling and provide EM coupling in the IR region.[2−6] The regular arrays of spherical metal nanoparticles (NPs), therefore, could enable improved nanoelectronic and photonic devices such as chemical and biosensors,[7,8] surface-enhanced Raman scattering (SERS) spectroscopy,[9] optical waveguides,[10] imaging,[11] and photovoltaic devices.[12] Dipole coupling of plasmon waves narrows extinction peaks and enhances EM fields up to 10^7 in spherical silver NP arrays relative to an isolated NP.[13] Regular arrays of gold NPs also exhibit strong, long-range interactions between particles that cannot be obtained in a disordered NP lattice.[14] SERS signal is amplified by varying particle shape, size, and interparticle spacing on the regular arrays of gold NPs.[15]

Diverse microfabrication techniques are being developed to meet rising demands for the fabrication of highly ordered metal NP arrays. Electron beam lithography (EBL),[16,17] nanoimprint lithography (NIL),[18] and focused ion beam (FIB) systems[19] have been used to produce periodic metal lattices of particular optical and geometrical interest. These methods are effective in creating high-resolution nanostructures with controllable size, shape, and spacing. However, they require expensive equipment for the lithography, ion etching, and metal deposition. In our previous works, it took ~36 h to fabricate 100 × 100 μm^2 regular arrays of gold NPs using a 1.2 million dollar EBL machine.[20,21] NIL and FIB also require long sample preparation times with expensive equipment. Electroless (EL) plating results in more cohesive particles with smaller particle size distributions than conventional top-down metal deposition, such as evaporation or sputtering.[20] In addition, top-down evaporation or sputtering limits particle shapes to cylindrical structures and precludes thermal shape transformation due to weak bonding between the metal film and structures. Emerging lithographic techniques using templates made of biological molecules,[22] such as DNA,[23,24] protein,[25] yeast cells,[26] or bacterial surface layers,[27] provide a biocompatible environment, but these templates are labile, and the resulting regular patterns of nanostructures are size-limited to a few nano- to micrometers.

Particle lithography, known as nanosphere lithography (NSL), is a simpler, more robust, and cost-effective means to create

*Address correspondence to dkroper@uark.edu.

Received for review February 18, 2010 and accepted June 15, 2010.

Published online June 21, 2010.
10.1021/nn100338f

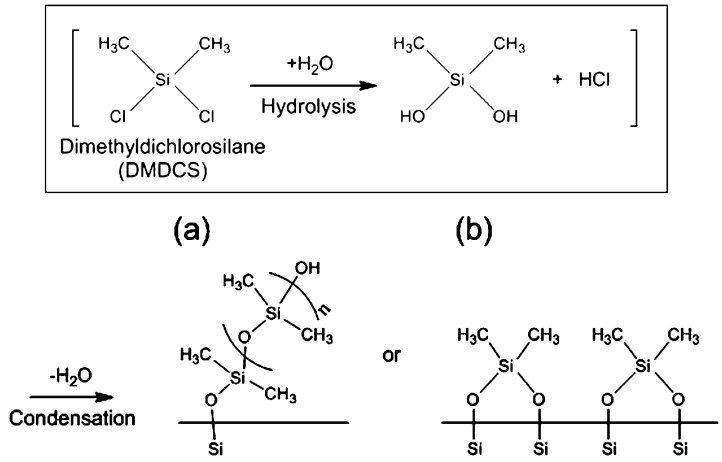

Figure 1. Silanization mechanism of dimethyldichlorosilane (DMDCS) on a quartz substrate: (a) vertical polymerization or (b) monolayer formation can result from condensation.

ordered two-[28] or three-dimensional[29] colloidal crystals which can be used as templates to fabricate metal nanostructures. Attractive capillary forces between monodispersed silica (Si) or polymer beads produce large areas of ordered colloidal crystals from millimeters to centimeters in scale.[30−32] Also, size and interparticle spacing of the metal NP array can be easily tuned by using different sizes of beads. Various shapes of metal nanostructures fabricated by NSL, such as triangles and spheres, have been characterized for use in localized surface plasmon resonance (LSPR) spectroscopy and SERS sensing.[33,34] However, although NSL has attracted much interest due to the above listed advantages over the other lithographic techniques, expensive and sophisticated metal deposition equipment is still required postlithography to produce ordered arrays of metal nanostructures. Chromium layers, which are often precoated to increase adhesion of the metal films during the metal vacuum deposition, are shown to be a limiting factor in the sensitivity of biological sensors.[35] Moreover, top-down metal deposition limits the diversity of the final array structure because the deposited metal films access only part of the interstitial areas between beads.

RESULTS AND DISCUSSION

Here, we present the first examination of gold film nanotemplating created using bottom-up EL plating on particle-lithographed silane layers. EL plating is an inexpensive, benchtop method to deposit diverse metals such as gold, silver, nickel, copper, and platinum on Si surfaces by chemical reduction of dissolved metal ions.[36] This report focuses on nanotemplating to produce *gold* structures using EL plating. We recently characterized EL-plated gold films deposited on flat quartz slides,[36] on inner walls of Si capillaries,[37] and on EBL-patterned indium−tin−oxide (ITO) glass substrates.[20,21] In each case, EL plating produced gold films of a predictable thickness and structure at a given deposition time. Island films may be transformed to gold NPs by thermal annealing. Strong attachment of the gold to the substrate upon extreme thermal, solvent, and EM exposures exhibits great potential of EL-plated nanostructures for bio/chemical sensing applications.

Surface modification of a quartz slide was performed with dimethyldichlorosilane (DMDCS) to prevent the interstitial surfaces between silica beads from being EL gold plated. DMDCS was selected as a silanizing agent due to its demonstrated effectiveness particularly for vapor phase reactions. Much greater water contact angles have been previously observed when surfaces were prepared in the vapor phase (θ_A/θ_R = 104°/103°, where θ_A and θ_R are advancing and receding contact angles) than surfaces made in solution (θ_A/θ_R = 92°/85°).[38] Additionally, DMDCS has greater vapor pressure and thermal stability, as well as a lower tendency to polymerize, compared to trichlorosilanes.[39] Due to its ultrahydrophobic character, reactions of alkylchlorosilanes with Si surfaces have been shown to generate hydrophobic coatings on micro/nanostructures,[40,41] antistiction layers on MEMS devices,[39] and water-repellent surfaces for self-cleaning purposes.[42] Surfaces coated with alkylchlorosilanes show different values in water contact angles and wettability depending on the number of chlorine atoms (mono-, di-, and trichlorosilanes) and the length of alkyl groups (methyl, ethyl, propyl, *etc.*).[38−40,43] However, alkylchlorosilane reaction mechanisms are all the same regardless of functionality.[39,44,45] First, Si−Cl bonds break to form Si−OH bonds, and HCl is produced with a trace amount of water, as shown in the case of DMDCS in Figure 1. HCl produced by this hydrolysis reaction does not interact with the Si surface or impede the silanization.[44] Second, the silanol groups can be covalently attached to the free hydroxyl (−OH) groups on the Si surface by condensation. During this reaction, di- and trichlorosilanes tend to polymerize vertically with available unbound silanol groups resulting in multilayer formation, as shown in Figure 1a.[38] A monolayer of DMDCS molecules can be also formed by binary covalent attachment in the absence of available unbound silanol groups, as shown in Figure 1b.[43] A

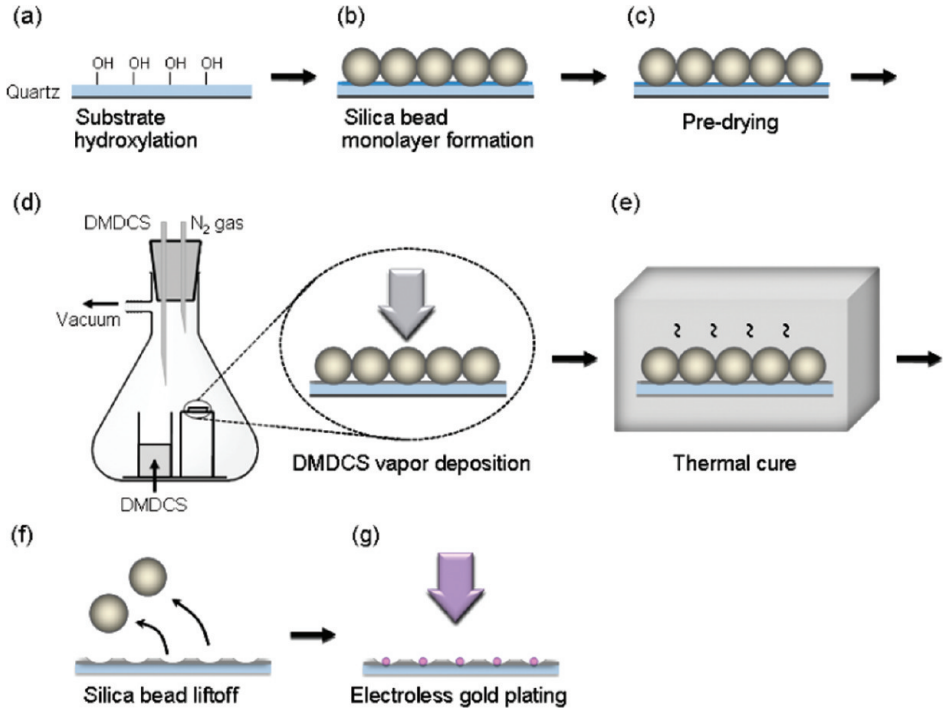

Figure 2. Schematic illustration of the procedure for the gold film nanotemplating.

detailed silanization reaction on the DMDCS-deposited silica bead monolayer is discussed in the description of Figure 4.

Figure 2 illustrates the gold film nanotemplating process used. Silica beads (1.81 ± 0.04 μm in diameter, 3 μL, 1%) were drop-coated onto piranha-hydroxylated quartz substrates (a,b) and, resulting silica bead monolayer samples were dried for 0−40 h on a 3D rocker platform in a 60% environmental chamber (c). The samples were then placed into a custom vacuum evaporation system to vapor-deposit DMDCS on the silica bead mask with deposition times ranging from 60 to 90 min (d). After DMDCS deposition, samples were incubated either in a 50 °C oven for 1−5 h to observe the effect of thermal curing on DMDCS condensation (e) or in a room temperature desiccator for 20 min as control samples. Next, silica beads were lifted off from the substrate in an ultrasonic water bath (f), and EL gold plating was performed on the particle-lithographed masks to produce nanotemplated structures (g). Details of the experimental procedures are included in the Experimental Section.

Figure 3 shows diverse nanotemplated gold film structures with increasing predrying times of the silica bead monolayer from (a) 0 min, (b) 30 min, (c) 15 h, to (d) 40 h at a constant DMDCS deposition time (60 min) and with no thermal cure. When the silica bead monolayer retained significant amounts of bulk liquid water between the beads, thick gold films were formed without making hexagonal array patterns, as shown in Figure 3a. As in the results from FTIR, quartz microbalance, and ellipsometric measurement, silane multilayer buildup (*e.g.*, vertical polymerization of DMDCS molecules) is because of liquid water traces left on the substrates.[43,46] Thus, gold island film can be plated onto free −OH ends of the polymerized DMDCS molecules *via* EL interactions without creating hexagonal array patterns. It was previously shown that an estimated EL deposition rate is ~8 nm/min during the first 4 min and is nonlinear afterward.[36] When the predrying time of the silica bead monolayer was increased to 30 min, however, uniform hexagonal arrays of silane ring structures appeared with an average outer ring diameter of 522.5 ± 29.7 nm (n = 42, where n is the number of counts). These silane ring structures appear as black rings in the SEM image. Corresponding hollow bars in the histogram of Figure 3b show their size distribution. Outside the silane ring areas, where water molecules are adsorbed on free Si surfaces, gold island film was plated onto available −OH groups of the polymerized DMDCS molecules *via* EL plating. Spherical gold NPs, appearing as white dots in the SEM image, corresponding to filled bars in the histogram of Figure 3b, were formed with an average diameter of 235.3 ± 32.6 nm (n = 51) at the center of each silane ring. When the silica bead monolayer was predried for 15 h, average diameters of the silane rings and spherical gold NPs were increased to 1116.9 ± 52.6 nm (n = 78) and 306.3 ± 34.7 nm (n = 67), respectively, with reduced areas of background gold film in Figure 3c. Increasing the predry time to 40 h produced similar diameters of the silane rings and spherical gold NPs to those of 15 h predried sample, 923.1 ± 72.1 (n = 65) and 321.0 ± 50.1 nm (n = 57), respectively, as shown in Figure 3d. Therefore, predrying was not performed longer than 40 h.

Morphology of gold NPs and island structures appears to result from different structures of water formed in three unique regions on Si surfaces adjacent to silica

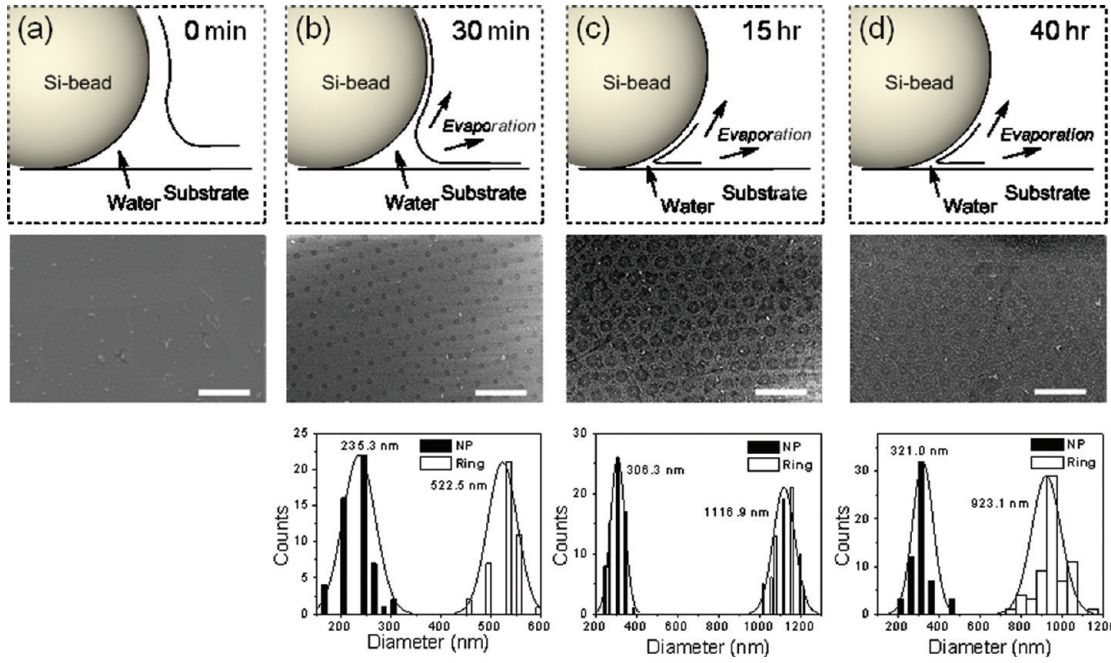

Figure 3. Schematic diagrams (first row), SEM images (second row), and histograms (third row) of the nanotemplated gold films prepared by predrying silica bead monolayer samples for (a) 0 min, (b) 30 min, (c) 15 h, and (d) 40 h in a 60% environmental chamber. Remaining water after each predrying was drawn in the schematics as solid water meniscus lines at bead−substrate interfaces. Scale bars in the SEM images are 5 μm. Average diameters of gold NPs at the center of each ring and outer diameters of silane rings are shown in filled and hollow bars in the histograms, respectively.

beads, as shown in Figure 4: (i) free surfaces, (ii) ≤10 nm cavities, and (iii) >10 nm cavities with menisci. On Si surfaces unbounded by adjacent surface structures (free surfaces), planar ice-like water structures grow up to ~3 molecular layers at relative humidity (RH) up to 30%.[47] In the RH range from 30 to 60%, a transitional region from ice-like to liquid water of ~1 molecular layer occurs, and liquid water begins to dominate on the top of this transitional region at RH > 60%.[47] However, when water adsorbs in cavities, as where Si substrate meets silica beads, ice-like structures persist up to ≤10 nm in cavity diameter.[48] Beyond 10 nm, water liquefies *via* capillary condensation between ice-like layers on cavity surfaces, forming a characteristic meniscus. Sorption isotherms in the region of capillary condensation exhibit sharp changes in adsorbed water content as well as hysteresis.[48−50] As water vapor pressure increases, an equilibrium plateau in adsorbed water is reached, during which water at the menisci edges adjacent to free surface evaporates and recondenses at the meniscus center, creating a dynamic circular pattern, as described in Figure 4.[51]

Comparing previously reported water structures with the results in Figure 3 suggests that DMDCS vapor near free surfaces is hydrolyzed by water vapor in equilibrium with free surface liquid. Hydrolyzed DMDCS vapor condenses with surface hydroxyls, resulting in silanization which is driven by the lower-energy state of

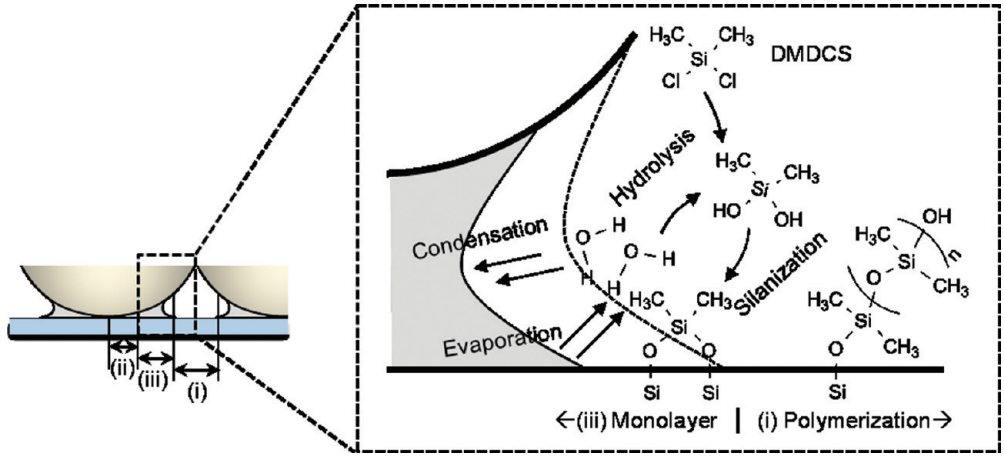

Figure 4. Schematic representation of DMDCS silanization in three different regions on Si surfaces adjacent to silica beads: (i) free surfaces, (ii) ≤10 nm cavities, and (iii) >10 nm cavities with menisci. A monolayer formation of DMDCS molecules on region (iii) and DMDCS polymerization on region (i) are shown in the close-up schematic on the right.

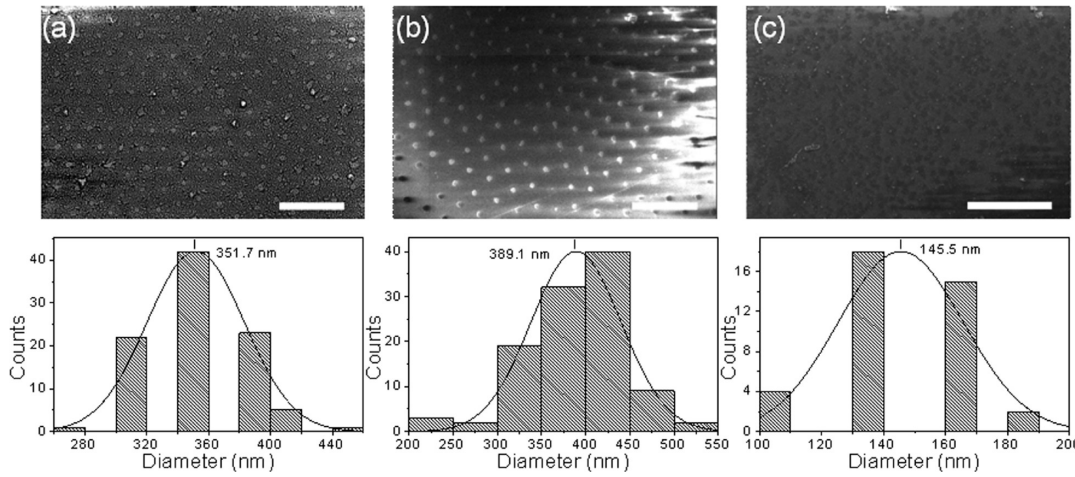

Figure 5. SEM images (first row) and histograms (second row) for the samples prepared after post-thermal cure for (a) 1, (b) 3, and (c) 5 h. Scale bars in the SEM images are 5 μm.

surface silanols. At ≤60% humidity, DMDCS covers free surfaces sparsely with an average degree of polymerization ≤4 (due to three ice-like and one transition water layer being present). This accounts for the dispersed gold island film appearing on free surface areas between silica beads after EL plating. In contrast, on surfaces of ≤10 nm cavities, silanization by DMDCS is precluded by steric inaccessibility, by lower water number density,[48] and by an intervening meniscus layer of liquid water. These cavity surfaces are exposed to EL plating solutions after lift-off of Si microbeads, which allows reduction of uniform gold island films that centered at the point where the microbead contacts the Si substrate. On >10 nm cavity surfaces, water evaporating from edges of associated menisci hydroxylates DMDCS vapor molecules that silanize surface hydroxyls, forming a uniform DMDCS monolayer that advances in the direction of the receding edge of the meniscus, until all liquid water has evaporated. This produces metal-free silane ring structures that have uniform diameters after 15−40 h of predrying time since dynamic equilibrium at the surface at 60% humidity has apparently been reached. Reduced predrying times (*e.g.*, 30 min) leave thicker menisci, which enhance vertical polymerization of DMDCS, associated with more difficult bead lift-off, thicker gold island films, and smaller silane ring structures.

Figure 5 shows SEM images and histograms of hexagonal arrays of spherical gold NPs created on a quartz substrate. Samples were prepared by thermally curing DMDCS-deposited silica bead monolayers in a closed-door 50 °C oven for (a) 1, (b) 3, and (c) 5 h at a constant predrying time (30 min) and DMDCS vapor deposition time (60 min). Temperature for the thermal cure was chosen to be 50 °C, which gives sufficient thermal energy to promote DMDCS condensation below the boiling temperature of DMDCS (70 °C). Temperatures much lower than 50 °C would have minimal thermal effects on DMDCS condensation, whereas temperatures much higher than 50 °C disrupt DMDCS layers silanized on the Si surface. In contrast to the results in Figure 3, silane rings did not appear in these samples and background gold films were not visible after 3 h of thermal curing. Average diameters of gold NPs were (a) 351.7 ± 31.5 (n = 94), (b) 389.1 ± 51.1 (n = 107), and (c) 145.5 ± 20.2 nm (n = 39) as shown in the histograms. Note that gold NPs in Figure 5b appeared to have sphericity ~1:1 with a height comparable to the width. Tilted SEM images provided NP sphericity as well as NP height information.[20] In previous reports, atomic force microscope (AFM) images of gold NPs showed reasonable agreement with SEM images.[36] However, AFM was less reliable than SEM primarily due to convolution between probe tip and particle structures. Reduced NP diameters and non-uniform background silane layers seen in Figure 5c were thought to be due to a disruption of hydrophilic layers on the substrate by an excessive 5 h thermal cure. Therefore, thermal cure was not applied longer than 5 h.

Characteristics of water molecules on Si surfaces and images including those shown in Figures 3 and 5 suggest that the thermal cure accelerates water condensation between adjacent DMDCS molecules silanized on free surfaces and on surfaces of cavities >10 nm, increasing surface hydrophobicity. This is consistent with reports that Si gel modified with γ-aminopropyltriethoxysilane and thermally cured at 150 °C showed minimum hydrolysis and polymerization in diffuse reflectance infrared Fourier transform spectra.[52] Attenuated total reflectance infrared spectroscopy has been used to show that highly hydrophobic silicon oxide surfaces, such as those covered with octadecyltrichlorosilane self-assembled monolayers (contact angle of water = 95 ± 5°), form primarily ice-like water structures.[53] On a superhydrophobic quartz surface modified with polymethylsiloxane (contact angle of water = 164 ± 2°), water molecules exhibited characteristics of free OH that are typically observed at air−water interfaces in vibrational sum frequency generation spectroscopy.[54] In Figure 5b, thermal cure appears to eliminate free surface silanol groups by dehydration, making them unavailable for EL gold plating,

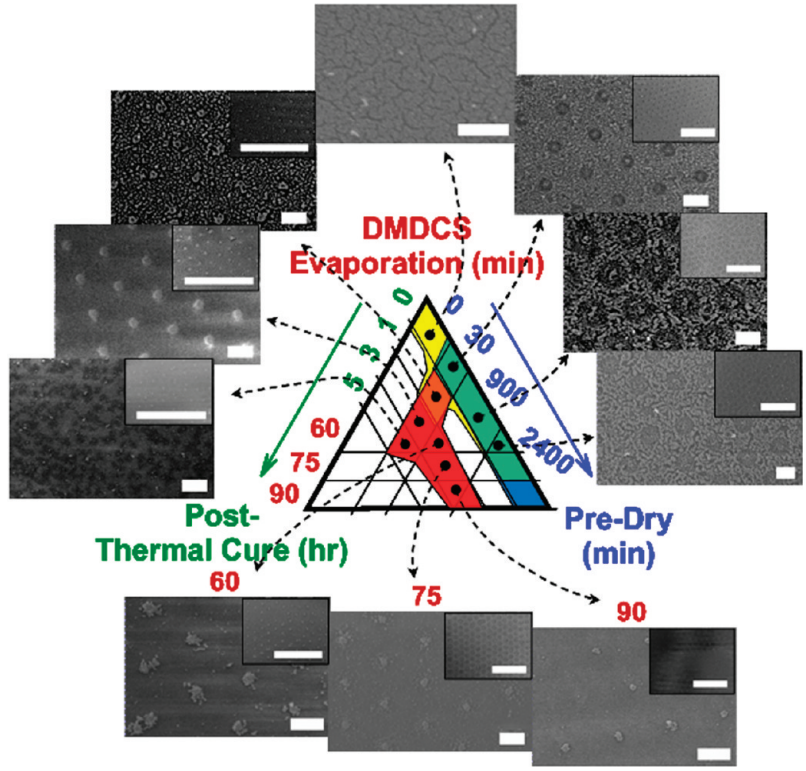

Figure 6. Triangle diagram of the nanotemplated gold films with three main experimental variables: (i) predry time (0−40 h), (ii) DMDCS evaporation time (60−90 min), and (iii) post-thermal cure time (0−5 h). Scale bars are 1 μm in the main SEM images and 10 μm in the inset SEM images.

and producing ultrahydrophobic character. Further characterization of adsorbed water on nanotemplated Si surfaces using spectroscopic techniques beyond what has been reported[52−54] is the subject of the future investigation. However, during gold plating, a high water contact angle was observed, consistent with reported values for DMDCS, $\theta_A/\theta_R = 104°/103°$.[38] After gold plating, the substrate was slightly reddish and transparent. Incomplete thermal cure, however, allows thin gold film to remain on the background surface, as shown in Figure 5a. In this case, sensitizing tin atoms make additional bonds to the active −OH ends of the DMDCS molecules.

The present gold film nanotemplating approach uses bottom-up, wet chemical reduction and galvanic replacement of metal ions dissolved in aqueous solutions to nanofabricate diverse structures based on the ultrahydrophobic nature of DMDCS. Unlike top-down metal deposition techniques, such as sputtering and evaporation, which can create shapes like crescents[55] or triangles[56] based on an angle of incidence due to shadowing, a solution-based EL plating results in angle-independent, uniform metal deposition. After thermal treatments, no other shapes have been observed except rounded gold NPs in previous reports.[20,21] Suspended gold NPs were recently reported to attach to particle-lithographed organosilane nanopatterns using thiol functionalization.[57] By comparison, the nanotemplating approach taken here does not require either chemical functionalization of the surface to bind NP or long time delays required to allow NPs to deposit. Moreover, the spherical NPs resulting from the present method produce more uniform optical responses than irregularly shaped clusters of gold NPs reported to attach to particle-lithographed organosilane nanopatterns using thiol functionalization.[57]

Figure 6 summarizes nanotemplated metal array structures in a triangle diagram with the three main experimental variables: (i) predry time (0−40 h), (ii) DMDCS evaporation time (60−90 min), and (iii) post-thermal cure time (0−5 h). Inset SEM images show typical nanotemplating structures for each in a lower magnification. Predry and thermal cure time were the most influential variables in determining shapes and dimensions of the nanostructures because they control the mass and structure of surface-associated water available for the DMDCS silanization. The background gold films, shown in yellow in the triangle diagram, became thinner when the samples were predried long enough to make the silane ring structures (in the blue color direction in the diagram) or when the samples were thermally cured for a long enough time to facilitate water condensation (the red color direction). Templating with smaller silica bead sizes increases background gold film at DMDCS evaporation times, which are comparable and lower. Using silica beads with a diameter of 1.8 μm, reducing DMDCS evaporation time from 90 to 60 min produced arrays of slightly smaller Au NP film islands with negligible background gold film in each case. However, using silica beads with a diameter of

690 nm resulted in background gold film between hexagonal arrays of gold NPs, which persisted at 15−19 h of predry and 3 h of thermal cure, even after DMDCS evaporation time was decreased from 75 to 45 min (data not shown). When the diameters of the silica bead were decreased from 1.8 μm to 690 nm, the average diameters of gold NPs were decreased from 328.4 ± 42.1 to 195.7 ± 16.0 nm, while other experimental conditions remained constant at 15 h predry, 75 min DMDCS vapor deposition, and 3 h thermal cure. This is consistent with a reported expression for a contact area of a sphere on a flat surface: $a = (RF/K)^{1/3}$, where a is radius of sphere contact area, R is sphere radius, F is externally applied loading force, and K is effective elastic modulus constant.[58] A ratio of the experimentally determined radii of gold NPs created using 1.8 μm and 690 nm gives $a/a' = 328.4/195.7 = 1.7$. This is in good agreement with the cube root of the ratio of the silica bead radii, $(R/R')^{1/3} = (1.8/0.69)^{1/3} = 1.4$.

To show uniformity and scalability of the regular array pattern, SEM images of the sample prepared after 15 h predry, 75 min DMDCS vapor deposition, and 3 h thermal cure are shown in Figure 7. Hexagonal arrays of silane ring structures that appear as black rings in Figure 7a arise from DMDCS monolayer formation that takes place preferentially on >10 nm cavity surfaces upon dynamic water evaporation, as described in Figure 4. Outside the silane ring areas, the white background in Figure 7a appears to have thinner silane layers than the silane ring areas to preclude gold atoms attaching to the substrate, as clearly shown in magnified SEM images in Figure 7b,c. Hexagonal arrays of spherical gold NPs with an average diameter of 300.2 ± 31.1 nm ($n = 55$) were observed with no background gold film. The total dimension of the hexagonal arrays of spherical gold NPs ranged up to millimeter size. Uniformity and regularity of the metal NP array produced by the present nanotemplating method are expected to allow potential applications in fabricating plasmonic,[59−61] sensing,[62,63] and imaging devices[64,65] that exhibit extraordinary EM enhancements.

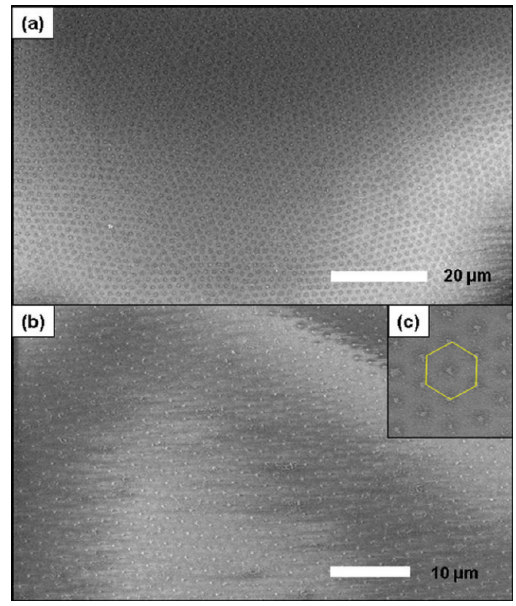

Figure 7. SEM images of the sample prepared after 15 h predry, 75 min DMDCS vapor evaporation, and 3 h thermal cure. Hexagonal arrays of gold NPs with an average diameter of 300.2 ± 31.1 nm ($n = 55$) are shown in a large area with no background gold film. Background features are better observed in magnified SEM images (b,c).

CONCLUSIONS

In summary, a novel nanotemplating method was reported to create regular arrays of silane rings or spherical gold NPs on Si substrates *via* selective EL plating on particle-lithographed silane layers. By controlling availability of surface-associated water during silanization, shapes and dimensions of the produced nanostructures were successfully tuned in agreement with a proposed silanization reaction on the DMDCS-deposited silica bead monolayer. The area of background gold film was decreased in a drier silica bead sample, as silane ring diameters were increased from 522.5 ± 29.7 to 1116.9 ± 52.6 nm. Background gold films then completely disappeared after 3 h of 50 °C thermal cure leaving only hexagonal arrays of spherical gold NPs with an average diameter of 389.1 ± 51.1 nm. This new nanotemplating technique, which eliminates the need for large, expensive lithography and metal deposition equipment, can reproducibly produce uniform metal NP arrays over large areas to improve potential capabilities of enhanced spectral features in opto-plasmonic devices.

EXPERIMENTAL SECTION

Quartz substrates (5 × 5 mm^2; GE 124 fused quartz, Chemglass Inc., Vineland, NJ) were immersed in a 120 °C piranha solution (concentrated H_2SO_4/30% H_2O_2 = 3:1 vol; Warning: piranha solution is potentially explosive and can cause skin burns) for 20 min to remove organic matter and to hydroxylate the substrate surface. After cooling, piranha solution was rinsed from the substrates with 200 mL of distilled, deionized water (D^2-H_2O) three times and stored in clean D^2-H_2O for 1 h to eliminate potential residual sulfur particles after the piranha cleaning.[66] Substrates were then dried in a controlled environmental chamber at constant humidity ($H = 61.0 \pm 0.2\%$), temperature ($T = 25.1 \pm 0.1$ °C), and pressure ($P = 0.9$ atm). The silica bead monolayer was formed by placing 3 μL of 1% silica bead suspension (1.81 ± 0.04 μm in diameter; Bangs Laboratories Inc., Fishers, IN) on these hydroxylated substrates. We found silica beads self-assemble into a close-packed monolayer with fewer defects when substrates are placed at the center of a 3D rocker incubator (Bellco Glass Inc., Vineland, NJ) at a speed of 0.11 rpm with an 8° tilt angle in the environmental chamber. After completing bead monolayer formation, substrates were further incubated (predried) in the environmental chamber for 0−40 h to test the influence of water content on silanization.

DMDCS vapor deposition on the silica bead monolayer was subsequently carried out in a custom vacuum evaporation system shown in Figure 2. Samples were placed on top of an inverted polystyrene tube in a 50 mL Erlenmeyer flask, then vacuum was pulled while circulating ultrapure N_2 gas for 30 s us-

ing a syringe needle inserted through a rubber stopper sealed using vacuum grease. The vacuum was temporarily halted by clamping the hose to slightly overpressure the flask with ultrapure N_2 gas and to fill another polystyrene tube with 1 mL of DMDCS (Sigma, St. Louis, MO) using a second syringe needle inserted through the rubber stopper. The clamp was released, and the vacuum condition was maintained for 60−90 min to vapor-deposit DMDCS on the bead monolayer substrates. When the DMDCS vapor deposition was finished, the vacuum hose was clamped and the flask was overpressured again with ultrapure N_2 gas to avoid sudden air rush into the flask as the stopper was opened. DMDCS-deposited samples were then either immediately incubated in a 50 °C oven in a closed brown glass jar (volume ~70 mL) for 1−5 h to expedite water condensation between adjacent DMDCS molecules silanized on Si surfaces or incubated in a room temperature desiccator for 20 min to determine effects of water in the hydrolysis only, without water condensation by the thermal cure. The silica beads were then removed by 5 s of ultrasonic vibrations, leaving available spots of hydroxyl (−OH) groups at contact points with the substrate where silica beads were arrayed hexagonally. Selective EL gold plating was then performed by three steps of a metal deposition on the substrates: immersion in a solution of (i) tin (Sn^{2+}) for 3 min, (ii) ammoniacal silver nitrate ($AgNO_3$) for 2 min, and (iii) sodium gold sulfite ($Na_3[Au(SO_3)_2]$) for 2.5−5 min. The strong hydrophobic character of methyl ($-CH_3$) groups on silanized monolayers of DMDCS blocked metal deposition by EL plating on interstitial areas between silica beads depending on the quality of silanization (see text for details). The substrates were washed with distilled, deionized, degassed water (D^3-H_2O) between each metal plating without drying them with ultrapure N_2 gas, and the final gold film nanotemplating structures were obtained.

Acknowledgment. This work was supported in part by NSF CMMI-0909749, NSF CMMI-0941677, and University of Arkansas Foundation. The authors thank S. Whitmore in the Department of Chemical Engineering at the University of Arkansas and J. Park in the Department of Chemistry at the University of Utah for useful discussions on the organosilane chemistry, and P. Blake and A. Russell in the Department of Chemical Engineering at the University of Arkansas for review and discussion of the manuscript.

REFERENCES AND NOTES

1. Barth, J. V.; Costantini, G.; Kern, K. Engineering Atomic and Molecular Nanostructures at Surfaces. *Nature* **2005**, *437*, 671–679.
2. Lamprecht, B.; Schider, G.; Lechner, R. T.; Ditlbacher, H.; Krenn, J. R.; Leitner, A.; Aussenegg, F. R. Metal Nanoparticle Gratings: Influence of Dipolar Particle Interaction on the Plasmon Resonance. *Phys. Rev. Lett.* **2000**, *84*, 4721–4724.
3. Félidj, N.; Laurent, G.; Aubard, J.; Lévi, G.; Hohenau, A.; Krenn, J. R.; Aussenegg, F. R. Grating-Induced Plasmon Mode in Gold Nanoparticle Arrays. *J. Chem. Phys.* **2005**, *123*, 221103.
4. Haynes, C. L.; McFarland, A. D.; Zhao, L.; Van Duyne, R. P.; Schatz, G. C.; Gunnarsson, L.; Prikulis, J.; Kasemo, B.; Käll, M. Nanoparticle Optics: The Importance of Radiative Dipole Coupling in Two-Dimensional Nanoparticle Arrays. *J. Phys. Chem. B* **2003**, *107*, 7337–7342.
5. Linden, S.; Kuhl, J.; Giessen, H. Controlling the Interaction between Light and Gold Nanoparticles: Selective Suppression of Extinction. *Phys. Rev. Lett.* **2001**, *86*, 4688–4691.
6. Chu, Y.; Schonbrun, E.; Yang, T.; Crozier, K. B. Experimental Observation of Narrow Surface Plasmon Resonances in Gold Nanoparticle Arrays. *Appl. Phys. Lett.* **2008**, *93*, 181108.
7. Zhang, J.; Atay, T.; Nurmikko, A. V. Optical Detection of Brain Cell Activity Using Plasmonic Gold Nanoparticles. *Nano Lett.* **2009**, *9*, 519–524.
8. Roper, D. K.; Ahn, W.; Taylor, B.; Dall'Asén, A. G. Enhanced Spectral Sensing by Electromagnetic Coupling with Localized Surface Plasmons on Subwavelength Structures. *IEEE Sens.* **2010**, *10*, 531–540.
9. Smythe, E. J.; Kickey, M. D.; Bao, J.; Whitesides, G. M.; Capasso, F. Optical Antenna Arrays on a Fiber Facet for *In Situ* Surface-Enhanced Raman Scattering Detection. *Nano Lett.* **2009**, *9*, 1132–1138.
10. Maier, S. A.; Friedman, M. D.; Barclay, P. E.; Painter, O. Experimental Demonstration of Fiber-Accessible Metal Nanoparticle Plasmon Waveguides for Planar Energy Guiding and Sensing. *Appl. Phys. Lett.* **2005**, *86*, 071103.
11. Laurent, G.; Félidj, N.; Truong, S. L.; Aubard, J.; Lévi, G.; Krenn, J. R.; Hohenau, A.; Leitner, A.; Aussenegg, F. R. Imaging Surface Plasmon of Gold Nanoparticle Arrays by Far-Field Raman Scattering. *Nano Lett.* **2005**, *5*, 253–258.
12. Atwater, H. A.; Polman, A. Plasmonics for Improved Photovoltaic Devices. *Nat. Mater.* **2010**, *9*, 205–213.
13. Zou, S.; Schatz, G. C. Silver Nanoparticle Array Structures That Produce Giant Enhancements in Electromagnetic Fields. *Chem. Phys. Lett.* **2005**, *403*, 62–67.
14. Auguié, B.; Barnes, W. L. Diffractive Coupling in Gold Nanoparticle Arrays and the Effect of Disorder. *Opt. Lett.* **2009**, *34*, 401–403.
15. Félidj, N.; Lau Truong, S.; Aubard, J.; Lévi, G.; Krenn, J. R.; Hohenau, A.; Leitner, A.; Aussenegg, F. R. Gold Particle Interaction in Regular Arrays Probed by Surface Enhanced Raman Scattering. *J. Chem. Phys.* **2004**, *120*, 7141–7146.
16. Komanicky, V.; Iddir, H.; Chang, K.; Menzel, A.; Karapetrov, G.; Hennessy, D.; Zapol, P.; You, H. Shape-Dependent Activity of Platinum Array Catalyst. *J. Am. Chem. Soc.* **2009**, *131*, 5732–5733.
17. Javey, A.; Dai, H. Regular Arrays of 2 nm Metal Nanoparticles for Deterministic Synthesis of Nanomaterials. *J. Am. Chem. Soc.* **2005**, *127*, 11942–11943.
18. Martensson, T.; Carlberg, P.; Borgstrom, M.; Montelius, L.; Seifert, W.; Samuelson, L. Nanowire Arrays Defined by Nanoimprint Lithography. *Nano Lett.* **2004**, *4*, 699–702.
19. Nagpal, P.; Lindquist, N. C.; Oh, S.; Norris, D. J. Ultrasmooth Patterned Metals for Plasmonics and Metamaterials. *Science* **2009**, *325*, 594–597.
20. Blake, P.; Ahn, W.; Roper, D. K. Enhanced Uniformity in Arrays of Electroless Plated Spherical Gold Nanoparticles Using Tin Presensitization. *Langmuir* **2010**, *26*, 1533–1538.
21. Ahn, W.; Blake, P.; Shultz, J.; Ware, M.; Roper, D. K. Fabrication of Regular Arrays of Gold Nanospheres by Thermal Transformation of Electroless-Plated Films. *J. Vac. Sci. Technol., B* **2010**, *28*, 638–642.
22. Sotiropoulou, S.; Sierra-Sastre, Y.; Mark, S. S.; Batt, C. A. Biotemplated Nanostructured Materials. *Chem. Mater.* **2008**, *20*, 821–834.
23. Zhang, J.; Liu, Y.; Ke, Y.; Yan, H. Periodic Square-like Gold Nanoparticle Arrays Templated by Self-Assembled 2D DNA Nanogrids on a Surface. *Nano Lett.* **2006**, *6*, 248–251.
24. Zheng, J.; Constantinou, P. E.; Micheel, C.; Alivisatos, A. P.; Keihl, R. A.; Seeman, N. C. Two-Dimensional Nanoparticle Arrays Show the Organizational Power of Robust DNA Motifs. *Nano Lett.* **2006**, *6*, 1502–1504.
25. McMillan, R. A.; Paavola, C. D.; Howard, J.; Chan, S. L.; Zaluzec, N. J.; Trent, J. D. Ordered Nanoparticle Arrays Formed on Engineered Chaperonin Protein Templates. *Nat. Mater.* **2002**, *1*, 247–252.
26. Chia, S.; Urano, J.; Tamanoi, F.; Dunn, B.; Zink, J. I. Patterned Hexagonal Arrays of Living Cells in Sol−Gel Silica Films. *J. Am. Chem. Soc.* **2000**, *122*, 6488–6489.
27. Mertig, M.; Wahl, R.; Lehmann, M.; Simon, P.; Pompe, W. Formation and Manipulation of Regular Metallic Nanoparticle Arrays on Bacterial Surface Layers: An Advanced TEM Study. *Eur. Phys. J. D* **2001**, *16*, 317–320.
28. Denkov, N. D.; Velev, O. D.; Kralchevsky, P. A.; Ivanov, I. B.; Yoshimura, H.; Nagayama, K. Two-Dimensional Crystallization. *Nature* **1993**, *361*, 26.
29. Jiang, P.; Bertone, J. F.; Hwang, K. S.; Colvin, V. L. Single-Crystal Colloidal Multilayers of Controlled Thickness. *Chem. Mater.* **1999**, *11*, 2132–2140.
30. Jiang, P.; McFarland, M. J. Large-Scale Fabrication of Wafer-Size Colloidal Crystals, Macroporous Polymers and Nanocomposites by Spin-Coating. *J. Am. Chem. Soc.* **2004**, *126*, 13778–13786.

31. Li, H.; Low, J.; Brown, K. S.; Wu, N. Large-Area Well-Ordered Nanodot Array Pattern Fabricated with Self-Assembled Nanosphere Template. *IEEE Sens. J.* **2008**, *8*, 880–884.
32. Pan, F.; Zhang, J.; Cai, C.; Wang, T. Rapid Fabrication of Large-Area Colloidal Crystal Monolayers by a Vortical Surface Method. *Langmuir* **2006**, *22*, 7101–7104.
33. Haynes, C. L.; Van Duyne, R. P. Nanosphere Lithography: A Versatile Nanofabrication Tool for Studies of Size-Dependent Nanoparticle Optics. *J. Phys. Chem. B* **2001**, *105*, 5599–5611.
34. Willets, K. A.; Van Duyne, R. P. Localized Surface Plasmon Resonance Spectroscopy and Sensing. *Annu. Rev. Phys. Chem.* **2007**, *58*, 267–297.
35. Haes, A. J.; Hall, W. P.; Chang, L.; Klein, W. L.; Van Duyne, R. P. A Localized Surface Plasmon Resonance Biosensor: First Steps toward an Assay for Alzheimer's Disease. *Nano Lett.* **2004**, *4*, 1029–1034.
36. Ahn, W.; Taylor, B.; Dall'Asén, A. G.; Roper, D. K. Electroless Gold Island Thin Films: Photoluminescence and Thermal Transformation to Nanoparticle Ensembles. *Langmuir* **2008**, *24*, 4174–4184.
37. Ahn, W.; Roper, D. K. Transformed Gold Island Film Improves Light-to-Heat Transduction of Nanoparticles on Silica Capillaries. *J. Phys. Chem. C* **2008**, *112*, 12214–12218.
38. Fadeev, A. Y.; McCarthy, T. J. Self-Assembly Is Not the Only Reaction Possible between Alkyltrichlorosilanes and Surfaces: Monomolecular and Oligomeric Covalently Attached Layers of Dichloro- and Trichloroalkylsilanes on Silicon. *Langmuir* **2000**, *16*, 7268–7274.
39. Ashurst, W. R.; Carraro, C.; Maboudian, R. Vapor Phase Anti-Stiction Coatings for MEMS. *IEEE Trans. Device Mater. Reliab.* **2003**, *3*, 173–178.
40. Öner, D.; McCarthy, T. J. Ultraphydrophobic Surfaces. Effects of Topography Length Scales on Wettability. *Langmuir* **2000**, *16*, 7777–7782.
41. Formanek, F.; Takeyasu, N.; Tanaka, T.; Chiyoda, K.; Ishikawa, A.; Kawata, S. Selective Electroless Plating To Fabricate Complex Three-Dimensional Metallic Micro/Nanostructures. *Appl. Phys. Lett.* **2006**, *88*, 083110.
42. Barberoglou, M.; Zorba, V.; Stratakis, E.; Spanakis, E.; Tzanetakis, P.; Anastasiadis, S. H.; Fotakis, C. Bio-Inspired Water Repellent Surfaces Produced by Ultrafast Laser Structuring of Silicon. *Appl. Surf. Sci.* **2009**, *255*, 5425–5429.
43. Rühe, J.; Novtny, V. J.; Kanazawa, K. K.; Clarke, T.; Street, G. B. Structure and Tribological Properties of Ultrathin Alkylsilane Films Chemisorbed to Solid Surfaces. *Langmuir* **1993**, *9*, 2383–2388.
44. Hair, M. L.; Hertl, W. Reactions of Chlorosilanes with Silica Surfaces. *J. Phys. Chem.* **1969**, *73*, 2372–2378.
45. Angst, D. L.; Simmons, G. W. Moisture Absorption Characteristics of Organosiloxane Self-Assembled Monolayers. *Langmuir* **1991**, *7*, 2236–2242.
46. Le Grange, J. D.; Markham, J. L.; Kurkjian, C. R. Effects of Surface Hydration on the Deposition of Silane Monolayers on Silica. *Langmuir* **1993**, *9*, 1749–1753.
47. Asay, D. B.; Kim, S. H. Evolution of the Adsorbed Water Layer Structure on Silicon Oxide at Room Temperature. *J. Phys. Chem. B* **2005**, *109*, 16760–16763.
48. Takei, T.; Mukasa, K.; Kofuji, M.; Fuji, M.; Watanabe, T.; Chikazawa, M.; Kanazawa, T. Changes in Density and Surface Tension of Water in Silica Pores. *Colloid Polym. Sci.* **2000**, *278*, 475–480.
49. Iiyama, T.; Ruike, M.; Kaneko, K. Structural Mechanism of Water Adsorption in Hydrophobic Micropores from *In Situ* Small Angle X-ray Scattering. *Chem. Phys. Lett.* **2000**, *331*, 359–364.
50. Beverley, K. J.; Clint, J. H.; Fletcher, P. D. I.; Thubron, S. Evaporation Rates of Water Contained within Porous Silica Particles. *Phys. Chem. Chem. Phys.* **1999**, *1*, 909–911.
51. Chamarthy, P.; Dhavaleswarapu, H. K.; Garimella, S. V.; Murthy, J. Y.; Wereley, S. T. Visualization of Convection Patterns near an Evaporating Meniscus Using μPIV. *Exp. Fluids* **2008**, *44*, 431–438.
52. Vranchen, K. C.; Van Der Voort, P.; Gillis-D'Hamers, I.; Vansant, E. F. Influence of Water in the Reaction of γ-Aminopropyltriethoxysilane with Silica Gel. *J. Chem. Soc., Faraday Trans.* **1992**, *88*, 3197–3200.
53. Asay, D. B.; Barnette, A. L.; Kim, S. H. Effects of Surface Chemistry on Structure and Thermodynamics of Water Layers at Solid−Vapor Interfaces. *J. Phys. Chem. C* **2009**, *113*, 2128–2133.
54. Asanuma, H.; Noguchi, H.; Uosaki, K.; Yu, H.-Z. Water Structure at Superhydrophobic Quartz/Water Interfaces: A Vibrational Sum Frequency Generation Spectroscopy Study. *J. Phys. Chem. C* **2009**, *113*, 21155–21161.
55. Shumaker-Parry, J. S.; Rochholz, H.; Kreiter, M. Fabrication of Crescent-Shaped Optical Antennas. *Adv. Mater.* **2005**, *17*, 2131–2134.
56. Haynes, C. L.; McFarland, A. D.; Smith, M. T.; Hulteen, J. C.; Van Duyne, R. P. Angle-Resolved Nanosphere Lithography: Manipulation of Nanoparticle Size, Shape, and Interparticle Spacing. *J. Phys. Chem. B* **2002**, *106*, 1898–1902.
57. Li, J.; Lusker, K. L.; Yu, J.; Garno, J. C. Engineering the Spatial Selectivity of Surfaces at the Nanoscale Using Particle Lithography Combined with Vapor Deposition of Organosilanes. *ACS Nano* **2009**, *3*, 2023–2035.
58. Schwarz, U. D. A Generalized Analytical Model for the Elastic Deformation of an Adhesive Contact between a Sphere and a Flat Surface. *J. Colloid Interface Sci.* **2003**, *261*, 99–106.
59. Maier, S. A.; Brongersma, M. L.; Kik, P. G.; Meltzer, S.; Requicha, A. G.; Atwater, H. A. Plasmonics—A Route to Nanoscale Optical Devices. *Adv. Mater.* **2001**, *13*, 1501–1505.
60. Bakker, R. M.; Yuan, H.; Liu, Z.; Drachev, V. P.; Kildishev, A. V.; Shalaev, V. M.; Pedersen, R. H.; Gresillon, S.; Boltasseva, A. Enhanced Localized Fluorescence in Plasmonic Nanoantennae. *Appl. Phys. Lett.* **2008**, *92*, 043101.
61. Zheng, Y. B.; Hsiao, V. K. S.; Huang, T. Active Plasmonic Devices Based on Ordered Au Nanodisk Arrays. *Proceedings of MEMS* **2008**, Tucson, AZ, USA, January 13−17, 705−708.
62. Rechberger, W.; Hohenau, A.; Leitner, A.; Krenn, J. R.; Lamprecht, B.; Aussenegg, F. R. Optical Properties of Two Interacting Gold Nanoparticles. *Opt. Commun.* **2003**, *220*, 137–141.
63. Pompa, P. P.; Martiradonna, L.; Della Torre, A.; Della Sala, F.; Manna, L.; De Vittorio, M.; Calabi, F.; Cingolani, R.; Rinaldi, R. Metal-Enhanced Fluorescence of Colloidal Nanocrystals with Nanoscale Control. *Nat. Nanotechnol.* **2006**, *1*, 126–130.
64. Bakker, R. M.; Drachev, V. P.; Yuan, H.; Shalaev, V. M. Enhanced Transmission in Near-Field Imaging of Layered Plasmonic Structures. *Opt. Express* **2004**, *12*, 3701–3706.
65. Salerno, M.; Krenn, J. R.; Lamprecht, B.; Schider, G.; Ditlbacher, H.; Felidj, N.; Leitner, A.; Aussenegg, F. R. Plasmon Polaritons in Metal Nanostructures: The Optoelectronic Route to Nanotechnology. *Opto-Electron. Rev.* **2002**, *10*, 217–224.
66. Clews, P. J.; Nelson, G. C.; Matlock, C. A.; Resnick, P. J.; Adkins, C. L. Minimizing Surfur Contamination and Rinse Water Volume Required Following a Sulfuric Acid/Hydrogen Peroxide Clean by Performing a Chemically Basic Rinse. *J. Proc. Electrochem. Soc.* **1997**, 23–28.